JOURNAL OF GEOPHYSICAL RESEARCH, VOL. 93, NO. C9, PAGES 10,782-10,796, SEPTEMBER 15, 1988

NONRESONANT AND RESONANT REFLECTION OF LONG WAVES IN VARYING CHANNELS

James T. Kirby and Padmaraj Vengayil[1]

Coastal and Oceanographic Engineering Department, University of Florida, Gainesville

Abstract. One of the principal drawbacks associated with the use of equations of Korteweg-deVries (KdV) or Kadomtsev-Petviashvili (K-P) form to model wave propagation in a varying channel is the implicit neglect of reflection in those equations. This study formulates pairs of KdV or K-P equations which are coupled through inhomogeneity in bottom slope or channel width, and applies these equations to several propagation problems involving aperiodic and periodic wave motion. The formulation eliminates the neglect of reflection effects in the single KdV or K-P equation approach. Forms of the KdV equations are given which totally account for mass flux balance between the incident and reflected wave. We then examine several cases involving waves propagating in variable channels and compare model results to previously available data.

1. Introduction

Evolution equations for weakly dispersive waves in the form of the Korteweg-deVries (KdV) or Boussinesq equations have long been known to be reasonably good predictors of wave form and propagation in channels of uniform and shallow depth, with the Boussinesq equations being able to describe general two-dimensional (in plan) motions but the KdV equation or its variants being limited to strictly one-dimensional, one-way propagation. Recently, the weakly two-dimensional equation of Kadomtsev and Petviashvili [1970] (K-P), which describes nearly one-dimensional propagation with weak transverse modulation, has been added to the arsenal of equations describing uniform depth motion.

Recently, interest in shallow water wave motion has been extended to the consideration of shoaling and other effects due to propagation in an inhomogeneous domain. This interest has lead to a number of variable depth extensions to the evolution equations listed above. Peregrine [1967] has provided a variable depth extension to the Boussinesq equations which allows for the shoaling and reflection of waves incident on a bottom slope. Peregrine's and other equations of similar form may be regarded as general models for two-dimensional propagation in regions of gradually varying depth. Variable depth forms of the KdV equation have also been developed which similarly allow for shoaling effects in one-dimensional propagation; a relevant form of equation of this type is chosen for this study from the work of Svendsen and Buhr Hansen [1978]. Liu et al. [1985] have similarly provided a variable depth form of the K-P equation and have applied that equation to the study of wave focusing and refraction by variable topography; a derivation of the variable-depth K-P equation appearing in that study is given here.

Despite their usefulness in describing the evolution of the dominant incident wave over topography, the KdV and K-P equations are considered by a number of investigators to be flawed, since the reflected wave is implicitly neglected and hence may be constructed only after identification of a mass sink in the incident wave, which then serves as a source for the reflected wave calculation [Miles, 1979; Knickerbocker and Newell, 1985]. The purpose of this study is to derive a set of coupled evolution equations for incident and reflected waves which account for mass exchange directly, and thus restore the direct applicability of the KdV and K-P equations in regions where strong reflection may significantly affect wave evolution.

In section 2 we outline a scheme for constructing coupled equations of KdV or K-P form using a heuristic approach based on the method of operator correspondence. Domain inhomogeneity is limited to variations in still water depth. In section 3 we turn our attention to propagation in channels and extend the KdV form of the equation to include variations in channel width as well as depth. Development of the model equations in mass-conserving form is considered in section 4. In section 5 the ability of the model to predict reflection is tested by comparison with the previous results of Goring [1978], who studied transmission and reflection of solitary waves at a sloping step. In section 6, examples of the scattering of a solitary wave in a channel with gradually varied width are given, and the influence of mass balance effects on wave evolution in the study of Chang et al. [1979] are investigated. Finally, in section 7 we turn to the problem of scattering of periodic waves by periodic bottom disturbances, and extend the study of the gradual reflection of a cnoidal wave by a sinusoidal bed started recently by Yoon and Liu [1987]. Two-dimensional calculations based on the K-P forms of the model equations will be reported separately.

2. Reflection From Varying Bottom Topography

The goal of this section is to derive a set of coupled equations of KdV or K-P type to model the forward-scattered and backscattered wave trains in a variable domain and to describe the exchange of energy between the waves due to interaction with bottom topography. The derivation is based on heuristic arguments and is aided by several key points. First, we neglect nonlinear interactions between incident and reflected waves to the order of terms considered. In particular, consideration

[1] Now at Civil Engineering Department, Massachusetts Institute of Technology, Cambridge.

Paper number 8C0415.
0148-0227/88/008C-0145$05.00

of the three-wave resonance conditions for opposite going periodic waves shows that no resonant interaction takes place between the waves at the order of quadratic nonlinearity. For the different case of aperiodic waves such as solitary waves, previous results (Maxworthy [1976] and Su and Mirie [1980], among others) have documented a phase-shifting, nonlinear interaction between colliding solitary waves. The present formulation neglects this possibility, which should not be of importance in the present study of reflection because of the expected smallness of the reflected wave, $O(\varepsilon\alpha)$, relative to the incident wave at $O(\varepsilon)$, where α characterizes a bottom slope or channel width variation. (The case of resonant reflection of periodic waves represents reflection $\rightarrow O(\varepsilon)$; however, the conclusion on three-wave interactions covers this case.)

The scaling for weakly nonlinear, weakly dispersive shallow water waves in a varying domain is

$$O(\varepsilon) = O(\mu^2) = O(\alpha) << 1$$

where ε denotes nonlinear effects and is characterized by $\max(|\eta|/h)$, μ^2 denotes dispersive effects and is proportional to $\omega^2 h/g$, and α characterizes maximum bottom slope. Further, η is the surface displacement, h is water depth, g is gravitational acceleration, and ω is a characteristic frequency. It is clear that under the scaling used here, nonlinear, dispersive, and wave-bottom coupling effects need only appear at leading order in equations involving all three effects. As a consequence, the coupling due to bottom slope effects may be derived directly from the nondispersive linear wave equation for variable depth, after which the terms describing nonlinearity and dispersion may be added in a consistent manner.

The method of operator correspondence is used to derive the set of coupled linear equations describing wave-bottom coupling effects. The general wave equation describing the propagation of linear, nondispersive waves over a variable topography is given by

$$\eta_{tt} - g\nabla_h \cdot (h\nabla_h \eta) = 0 \qquad (1)$$

where here η represents a general two-dimensional surface displacement. Substituting frequencies for time derivatives in (1) according to

$$\eta_t = -i\omega\eta; \qquad \omega = (gh)^{1/2} k = ck \qquad (2)$$

equation (1) is rewritten as

$$\eta_{xx} + \frac{h_x}{h}\eta_x + \gamma^2\eta = 0 \qquad (3)$$

where

$$\gamma^2\eta = \frac{\omega^2}{gh}\eta + \frac{1}{h}(h\eta_y)_y \qquad (4)$$

The surface displacement η is written as the sum of the displacements of the forward-scattered wave traveling in +x direction, η^+, and the backscattered wave traveling in −x direction, η^-. Coupled equations of the form

$$\eta_x^+ = i\gamma\eta^+ + F(\eta^+,\eta^-) \qquad (5a)$$

$$\eta_x^- = -i\gamma\eta^- - F(\eta^+,\eta^-) \qquad (5b)$$

are sought, where F is the desired unknown coupling function. Repeated substitution of (5) in (3) gives

$$F = -\frac{1}{2}\frac{(\gamma h)_x}{\gamma h}(\eta^+ - \eta^-) \qquad (6)$$

From (4), γ is a pseudo differential operator which may be approximated by binominal expansion if the following assumption holds:

$$\frac{1}{h}\frac{\partial}{\partial y}\left(h\frac{\partial}{\partial y}\right) << \frac{\omega^2}{gh} \qquad (7)$$

This indicates a restriction to small propagation angles with respect to the x direction. This restriction is analyzed (and the connection to the parabolic approximation is discussed) in Appendix A.

Using a binomial expansion, the general expression for γ is

$$\gamma = \frac{\omega}{c} + \frac{c}{2\omega h}\frac{\partial}{\partial y}\left(h\frac{\partial}{\partial y}\right) \qquad (8)$$

To leading order, γ is given by (from Appendix A)

$$\gamma = \frac{\omega}{c} + O(\theta^2) \qquad (9)$$

where θ denotes a necessarily small propagation direction with respect to the x axis, (we assume $\theta^2 = O(\varepsilon)$) and hence

$$\gamma_x \approx -\frac{\omega}{c^2}c_x = -\frac{\omega}{2c}\frac{h_x}{h} \qquad (10)$$

Using (9) and (10), equation (6) is rewritten as

$$F = -\frac{h_x}{4h}(\eta^+ - \eta^-) = -\frac{c_x}{2c}(\eta^+ - \eta^-) \qquad (11)$$

The coupled equations are obtained from (5) using the expressions for F and γ and are written together as

$$\eta_x^\pm = \pm\frac{i\omega}{c}\eta^\pm \mp \frac{c_x}{2c}(\eta^+ - \eta^-) \pm \frac{ic}{2\omega h}(h\eta_y^\pm)_y \qquad (12)$$

Inverting the operator form of the $i\omega\eta^\pm$ terms and further using ω=kc in the y derivative terms, (12) is written as

$$\pm ik \{\eta_t^\pm \pm c\eta_x^\pm + \frac{c_x}{2}(\eta^+ - \eta^-)\} = \mp \frac{1}{2c}(c^2\eta_y^\pm)_y \tag{13}$$

Allowing 1/ik to correspond to an integral over x,

$$\frac{1}{ik}\eta^+ = \int_x \eta^+ dx \qquad \frac{1}{-ik}\eta^- = \int_x \eta^- dx \tag{14}$$

(13) may be rewritten as

$$\eta_t^\pm \pm c\eta_x^\pm + \frac{c_x}{2}(\eta^+ - \eta^-) \mp \int_x^\infty \frac{1}{2c}(c^2\eta_y^\pm)_y\, dx = 0 \tag{15}$$

This corresponds to the integro-differential form of the K-P equation, which has proven to be more convenient for numerical computations (see, for example, Katsis and Akylas [1987]). The set of coupled equations (15) represents linearized, nondispersive K-P equations describing incident and reflected wave fields which are linearly coupled through the bottom slope h_x.

It may be shown by back substitution that the set of linear nondispersive equations neglecting y derivatives are completely equivalent to the one-dimensional form of (1). Similar correspondence between (15) and the original model (1) does not exist, of course, because of the binomial approximation used. For the case of localized disturbances vanishing at $x \to \pm\infty$ together with their derivatives, summing the two components of (15) (neglecting y derivatives) and integrating from $-\infty$ to $+\infty$ gives

$$\frac{d}{dt}\int_{-\infty}^{\infty} \eta dx = 0 \tag{16}$$

The linear nondispersive reflection process thus conserves the total mass of displacement in the two wave trains.

The equations (15) may be extended to include weakly nonlinear, weakly dispersive effects. The variable depth KdV equation in stationary coordinates, given by Svendsen and Buhr Hansen [1978], may be written as

$$\eta_t + c\eta_x + \frac{c_x}{2}\eta + \frac{3c\eta\eta_x}{2h} + \frac{h^2c}{6}\eta_{xxx} = 0 \tag{17}$$

Equation (17) is valid for the scaling assumed here. The appropriate forms of the nonlinear term and linear dispersive term of (17) can be added directly to (15) to give the coupled equations for weakly nonlinear, weakly dispersive shallow water waves. Adding the appropriate terms in equations (15) gives the K-P type coupled evolution equations for nonlinear shallow water waves

$$\eta_t^\pm \pm c\eta_x^\pm + \frac{c_x}{2}(\eta^+ - \eta^-) \pm \frac{3c\eta^\pm\eta_x^\pm}{2h} \pm \frac{h^2c}{6}\eta_{xxx}^\pm$$

$$\mp \int_x^\infty \frac{1}{2c}(c^2\eta_y^\pm)_y\, dx = 0 \tag{18}$$

The variable depth K-P equation given by Liu et al. [1985] is obtained by neglecting the coupling in (18) and differentiating with respect to x. Further, neglecting y dependence yields the desired coupled KdV equations, while further neglecting coupling recovers (17) for the incident wave alone.

To the order of approximation assumed, spatial derivatives may be replaced by time derivatives in the linear dispersive terms to improve estimates of linear dispersion. We adopt a form of the equations incorporating one time derivative in the dispersive term, leading to equations analogous to the regularized long wave (RLW) equation of Peregrine [1966] and Benjamin et al. [1972]. The resulting model for one-dimensional propagation is then taken to be

$$\eta_t^\pm \pm c\eta_x^\pm + \frac{c_x}{2}(\eta^+ - \eta^-) \pm \frac{3c\eta^\pm\eta_x^\pm}{2h} - \frac{h^2}{6}\eta_{xxt}^\pm = 0 \tag{19}$$

We further note here that the form

$$\eta_x = \frac{i\omega}{c}\eta - \frac{c_x}{2c}\eta + \frac{ic}{2\omega h}(h\eta_y)_y \tag{20}$$

from (12) may be inverted twice in time to obtain

$$\eta_{tt} + c\eta_{xt} + \frac{c_x}{2}\eta_t = \frac{1}{2}(c^2\eta_y)_y \tag{21}$$

This is equivalent to the second approximation to a radiating boundary condition obtained by Engquist and Majda [1977], further extended to the case of variable depth.

3. Equations for a Gradually Varied Channel

Shuto [1974], among others, has considered an extension to the one-dimensional KdV equation for the case of waves propagating in a long channel of depth h(x) and half width b(x). Shuto's equation may be written in dimensional form and stationary coordinates as

$$b\eta_t + bc\eta_x + \frac{(bc)_x}{2}\eta + \frac{3bc}{2h}\eta\eta_x + \frac{bch^2}{6}\eta_{xxx} = 0 \tag{22}$$

The extension to Svendsen and Buhr Hansen's [1978] equation to account for varying channel width is readily apparent. In this section, we extend (22) to account for reflections from changes in channel width as well as depth.

Starting with the linear wave equation (7), we impose lateral boundary conditions

$$\eta_y - b_x\eta_x = 0 \qquad y = \pm b(x) \tag{23}$$

Integrating (1) from y=-b to b, applying Leibnitz rule, and assuming cross-channel variations of η

to be weak enough to ignore, we obtain an integrated wave equation given by

$$\eta_{tt} - \frac{1}{b}(ghb\eta_x)_x = 0 \quad (24)$$

Following the procedure of section 2, we expand (24) and employ operator correspondence in the time domain to obtain

$$\eta_{xx} + \frac{(bh)_x}{bh}\eta_x + \gamma^2\eta = 0 \quad (25)$$

where now γ^2 is given simply by

$$\gamma^2\eta = \frac{\omega^2}{gh}\eta \quad (26)$$

Employing the procedure of section 2 leads to coupled equations of the form (5) with $F(\eta^+,\eta^-)$ given by

$$F = -\frac{(bc)_x}{2bc}(\eta^+ - \eta^-) \quad (27)$$

Use of (27) in the coupled equations along with

$$\gamma\eta = \frac{\omega}{c(x)}\eta \quad (28)$$

then leads directly to the coupled linear equations

$$\frac{1}{c}\eta_t^\pm \pm \eta_x^\pm + \frac{(bc)_x}{2bc}(\eta^+ - \eta^-) = 0 \quad (29)$$

Assuming bottom slope and width changes to be small, we consistently add dispersive and nonlinear effects to obtain

$$b\eta_t^\pm \pm bc\eta_x^\pm + \frac{(bc)_x}{2}(\eta^+ - \eta^-) \pm \frac{3bc}{2h}\eta^\pm\eta_x^\pm \pm \frac{bch^2}{6}\eta_{xxx}^\pm = 0 \quad (30)$$

Neglecting coupling in each component equation of (30) leads to two separate equations of Shuto's type describing waves propagating in each direction in the channel. The coupling term implies that any varying channel whose variations maintain the constancy of bc is completely transparent to the passage of a wave, even though the wave itself undergoes evolution due to variations in h(x). As was the case with the results of section 2, the model equations (30) may be arbitrarily altered to RLW form.

4. Mass-Conserving Forms of the KdV Equations

The sets of coupled KdV equations (21) and (30) may be written in forms which lead to exact conservation of mass in the total wave system, to the level of the approximation used here, following the arguments of Miles [1979]. Rearranging the nonlinear and dispersive terms in (30) gives

$$(b\eta^\pm)_t \pm bc\eta_x^\pm + \frac{(bc)_x}{2}(\eta^+ - \eta^-) \pm \left\{\frac{3bc\eta^{\pm 2}}{4h} + \frac{bch^2}{6}\eta_{xxx}^\pm\right\}_x = O(\epsilon\alpha,\mu^2\alpha) \quad (31)$$

Terms appearing on the right-hand sides of (31) are formally small with respect to the present approximation and may be dropped, leaving the proposed mass-conserving form of the equation. Corresponding results for a channel of constant width follow by setting b = 1.

For the case of disturbances $\eta^\pm$ which vanish as $|x|\to\infty$, mass conservation in the total system follows simply by adding the component equations of (31) and then integrating over x, to obtain

$$\frac{d}{dt}\int_{-\infty}^{\infty} b(\eta^+ + \eta^-)\,dx = \frac{d}{dt}\int_{-\infty}^{\infty} b\eta dx = 0 \quad (32)$$

An alternate arrangement of equations (31) and integration from some fixed position x_0 to ∞ yields the relations

$$\frac{d}{dt}\int_{x_0}^{\infty}(b\eta^\pm)\,dx = \pm\tilde{Q}^\pm \pm \frac{1}{2}\int_{x_0}^{\infty}(bc)_x\eta dx \quad (33)$$

where

$$\tilde{Q}^\pm(x_0) = \left\{bc\eta^\pm + \frac{3bc\eta^{\pm 2}}{4h} + \frac{bch^2}{6}\eta_{xx}^\pm\right\}_{x_0} \quad (34)$$

represents flux of mass across station x_0 into $x > x_0$. The integral term on the right-hand side of (33) represents the sink or source of mass flux into or out of each wave system, which is seen to be equal and opposite in sign for each equation, indicating equivalence of interchanged mass in each subsection of the x interval. For the case of weak reflection, $O|\eta^-| \ll O|\eta^+|$, the integral on the right hand sides of (33) reduces to the approximate form

$$\int_x^{\infty}(bc)_x\eta dx \approx \int_x^{\infty}(bc)_x\eta^+ dx + O(\epsilon^2\alpha) \quad (35)$$

We note that Miles [1979], who analyzed Shuto's one-way equation, gave the mass flux $Q^+(x)$ as

$$Q^+(x) = \tilde{Q}^+(x) + \frac{1}{2}\int_x^{\infty}(bc)_x\eta^+ dx \quad (36)$$

and then identified the approximation in (35) as the principal source of mass to the reflected wave because of its dominance of the term $Q^+(x)$ as $x \to -\infty$. This interpretation arises naturally here through the analysis of the corresponding equation for the reflected wave motion, with the addition that the integral may be immediately identified as a source-sink mechanism without the intermediate analysis of residual fluxes. In

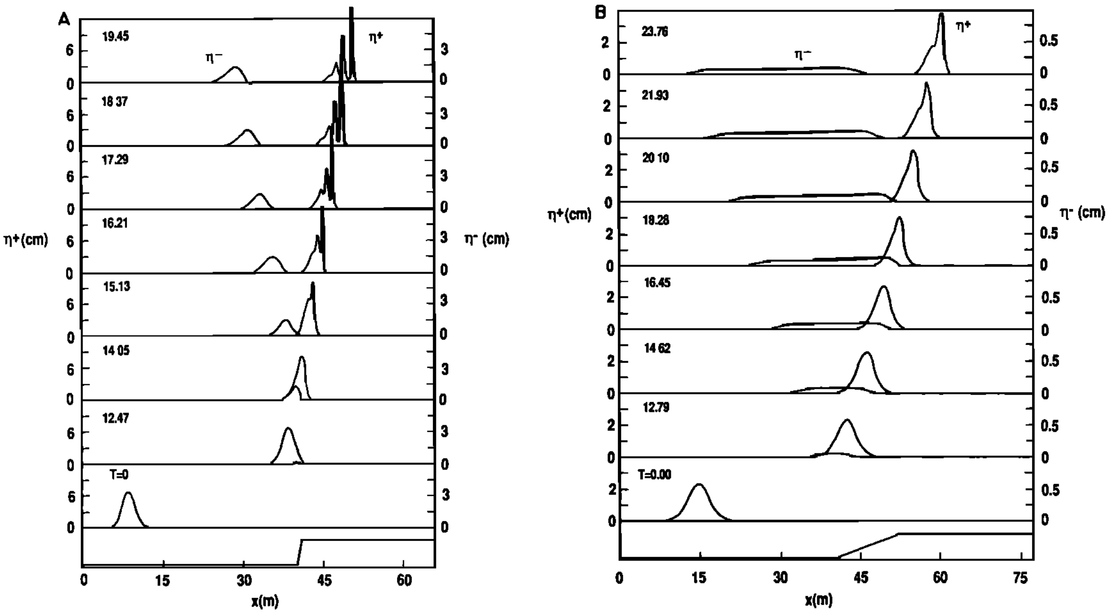

Fig. 1. Reflection and transmission of a solitary wave propagating onto a shelf. (a) $H_I/h_1 = 0.15$, $L/\ell = 0.5$, $h_1/h_2 = 3.0$. (b) $H_I/h_1 = 0.05$, $L/\ell = 4.0$, $h_1/h_2 = 3.0$.

addition, we obtain the complete feedback between the reflected and incident wave through the unapproximated form of (35).

In the following, we use the mass-conserving equations (31) written in RLW form, which gives

$$b\eta^{\pm}_{t} \pm bc\eta^{\pm}_{x} + \frac{(bc)_x}{2}(\eta^{+} - \eta^{-}) \pm \left(\frac{3bc\eta^{\pm 2}}{4h} \mp \frac{bh^2}{6}\eta^{\pm}_{xt}\right)_x = 0 \qquad (37)$$

The corresponding nonconservative forms are obtained from (30) after multiplying by bc. The numerical scheme used in the following two sections is a simple extension of the three-level, implicit scheme developed by Eilbeck and McGuire [1975], extended to account for variable coefficients. Details are omitted and may be found in the work of Vengayil and Kirby [1986] for the nonconservative forms of the RLW equations.

5. Solitary Waves Propagating Onto a Shelf

We first test the ability of the linear coupling mechanism to calculate reflection. An accurate set of measurements of reflections from a solitary wave propagating over a slope is available from the study of Goring [1978]. We consider waves of initial height H_I, in water of depth h_1, which propagate into water of depth h_2 over a linear transition of length L and slope $(h_1-h_2)/L$. The depth transitions considered here are fairly short ($L/\ell = O(1)$, where ℓ is a characteristic wave length) and the mass balance corrections discussed in the preceding section are not significant, with results of conservative and nonconservative calculations agreeing to within 1-2%.

5.1. Reflected Waves

The independent length scales involved in the reflection problem are the incident wave height H_I, upstream water depth h_1, downstream water depth h_2, and slope length L. The reflected wave height is given by H_R. A characteristic horizontal length ℓ of a solitary wave is completely defined by the incident wave height H_I and upstream depth h_1, and is defined by Goring [1978] as

$$\ell = 1.5\,(H_I/h_1)^{-1/2} h_1 \qquad (38)$$

The reflection process is characterized by three nondimensional parameters; the relative incident wave height, H_I/h_1, the length ratio L/ℓ, and the depth ratio, h_1/h_2. Choosing specific values for the nondimensional parameters L/ℓ and h_1/h_2 characterizes the slope as mild or steep.

In Figure 1a, an example of the propagation of an incident wave of $H_I/h_1 = 0.15$ over a fairly steep slope of $L/\ell = 0.5$ and $h_1/h_2 = 3$ is presented. As the wave propagates up the slope, a reflected wave similar in shape to the incident wave and nearly a fifth of the incident wave amplitude emerges. As it propagates on the shelf, the transmitted wave disintegrates into a series of solitary waves with the leading wave being the largest. The mildly sloping shelf shown in Figure 1b produces a reflected wave which is less peaked than the incident wave. The rear end of the wave shows a higher amplitude, indicating an increase in reflection as the incident wave moves up the slope. For this case, $L/\ell = 4.0$, $h_1/h_2 = 3$, and $H_I/h_1 = 0.05$. Goring [1978] presented an extensive study of the effect of the length ratio L/ℓ on the shape of the reflected wave. Results obtained in the present study are in excellent

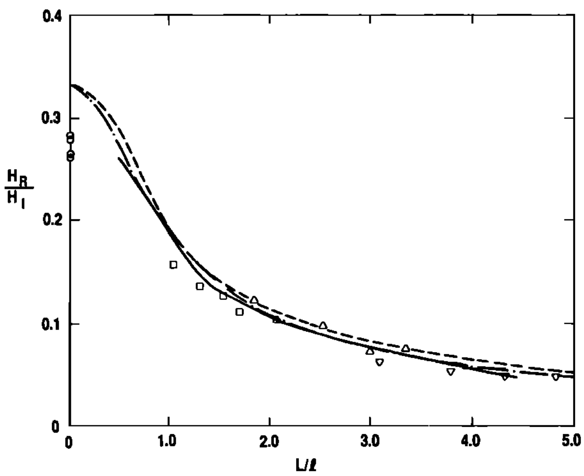

Fig. 2. Variation of reflection coefficient H_R/H_I with length ratio L/ℓ, for a depth ratio $h_1/h_2 = 4.0$. The solid line shows the present results, the dashed line shows Goring's [1978] nonlinear dispersive results, and the dashed-dotted line shows Goring's [1978] linear nondispersive results. Data from Goring [1978].

agreement with the results obtained by Goring [1978] using linear nondispersive theory.

In Figure 2, the reflection coefficient H_R/H_I is plotted as a function of the length ratio L/ℓ, for a solitary wave of $H_I/h_1 = 0.1$ and a depth ratio $h_1/h_2 = 4$. The reflection coefficients are compared with Goring's nonlinear dispersive and linear nondispersive theories and with his experimental results for various slopes and relative incident wave heights. The numbers next to the points indicate the values of the relative incident wave height H_I/h_1. Since the coupled evolution equations are valid only for mildly varying topographies, slopes with length ratio $L/\ell < 0.25$ are not considered. In all cases the present theory underpredicts the reflection coefficient when compared with Goring's nonlinear dispersive theory, but it is in reasonable agreement with results of Goring's linear nondispersive theory. The effect of the relative incident wave height on wave reflection is seen to be almost negligible from the results presented in Table 1, where reflections computed by the present method are compared with Goring's results obtained using linear nondispersive theory.

TABLE 1. Reflection Coefficients H_R/H_I for Various Length Ratios L/ℓ and Relative Incident Wave Heights H_I/h_1 for the Depth Ratio $h_1/h_2 = 3.0$

	H_I/h_1		
L/ℓ	0.05	0.10	0.15
0.53	0.214 (0.218)	0.212	0.212
1.03	0.151 (0.152)	0.155	0.155
1.56	0.108 (0.110)	0.106	0.111
2.00	0.088 (0.089)	0.087	0.095

Goring's [1978] linear results are given in parentheses.

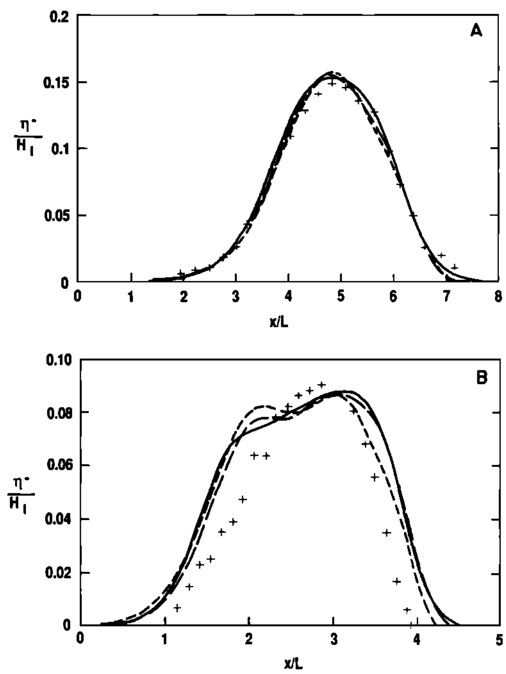

Fig. 3. Comparison of numerical reflected wave profiles with experimental results of Goring [1978] for (a) $L/\ell = 1$, and (b) $L/\ell = 2$. Numerical results are shown for —— $H_I/h_1 = 0.05$ (solid line), $H_I/h_1 = 0.10$ (long-dashed line), and -•-• $H_I/h_1 = 0.15$ (short-dashed line), and experimental results are shown for $H_I/h_1 = 0.0522$ (pluses).

In Figure 3 the predicted wave profile of the reflected wave is compared with experimental results of Goring. The amplitude of the reflected wave is normalized with respect to the incident wave height so that reflected waves corresponding to different incident wave heights can be compared directly. The experimental results are for a wave of $H_I/h_1 = 0.0522$ and numerical results are presented for three cases of $H_I/h_1 = 0.05$, 0.10, and 0.15. In Figure 3a the reflected waves from a slope ($L/\ell = 1.0$ and $h_1/h_2 = 3.0$) are compared with the experimental data and the agreement is fairly good, except at the crest. This discrepancy may be due to the neglect of friction in the numerical model. The results for a slope $L/\ell = 2.0$ and $h_1/h_2 = 3.0$, presented in Figure 3b, are not in agreement with the data, but the overall shape of the predicted wave is similar to the experimental data. Accuracy of measurement of the reflected waves, which are very small compared with the incident wave, may influence the shape of the wave considerably. In view of the close agreement in the profiles of waves of different relative wave amplitudes, it may be postulated that reflection may be considered to be a linear process dependent on the parameters L/ℓ and h_1/h_2 characterizing the slope, a view which was also put forward by Goring. These results support the use of the simple coupling mechanism assumed here.

5.2. Transmitted Waves

Results for evolution of the transmitted wave in the constant depth region beyond the slope

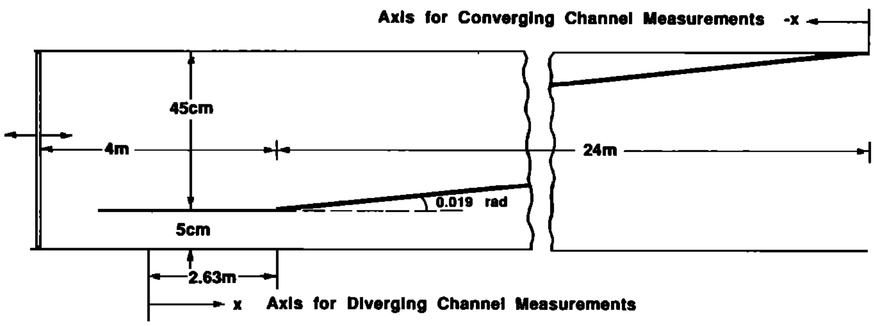

Fig. 4. Plan view of wave channel in experiments of Chang et al. [1979].

exhibit the usual features of disintegration into a train of several solitary waves and are not reproduced here. Numerical results for surface displacement were found to agree well with the experimental results presented by Goring. We remark here that the integrable property of the KdV equation in the transmitted-wave region would allow for a prediction of the number of solitons which evolve out of the wave computed at the top of the slope. No data are available to confirm or deny these predictions, so we have not pursued this question further.

6. Solitary Waves in Diverging and Converging Channels

We now consider a case of waves in a much more gradual transition, consisting of a linear variation in channel width. A comprehensive set of data is provided by Chang et al. [1979] (hereinafter referred to as CMM). Because of the slow variation of the channel width used here, reflection is of only minor importance in determining the height of the transmitted wave; however, the mass balance correction discussed in section 4 becomes quite important.

6.1. CMM Experiments

CMM measured the evolution of wave height of an initial solitary wave in both a diverging and a converging laboratory flume. A schematic of the channel geometries is given in Figure 4, which is adapted from Figure 1 of CMM. CMM measured waves for a range of initial wave heights and still water depths. The most detailed sets of results are for the cases of 20 cm depth in a diverging channel (three initial amplitudes [CMM, Figure 2]) and 30 cm depth in a converging channel (four initial amplitudes [CMM Figure 4]). Data consist of measured maximum $\eta(t)/h$ versus position along the channel. Reflections were not reliably measured. The data given by CMM are reproduced in Figures 5 and 6. CMM provided numerical computations based on the nonconservative form (equation (22)) further transformed to a coordinate system moving at the linear long-wave speed. For the case of the diverging channel, numerical results indicated asymptotic agreement with results for the adiabatic evolution of a solitary wave, which gives [Miles, 1979]

$$H(x) = H_0 \left(\frac{b(x)}{b_0}\right)^{-2/3} \tag{39}$$

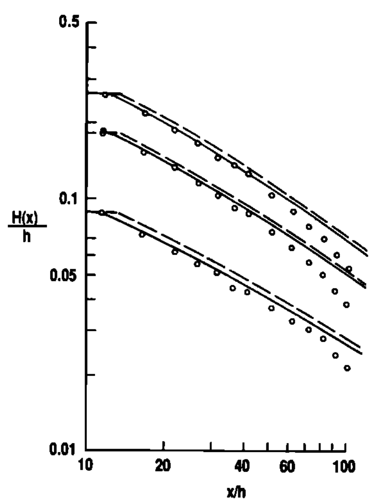

Fig. 5. Normalized amplitude of solitary waves in diverging channel with h = 20 cm and initial amplitudes H_0/h = 0.088, 0.185, and 0.259. Circles show data from CMM, solid lines show the total wave train, and dashed lines show the incident wave alone.

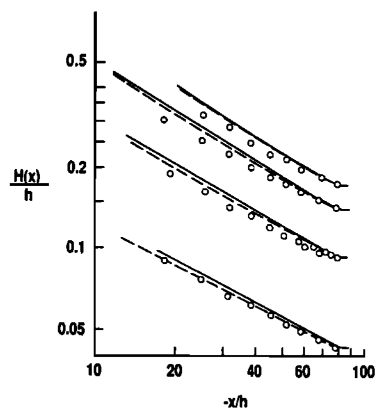

Fig. 6. Normalized amplitude of solitary waves in converging channel with h = 30 cm and initial amplitudes H_0/h = 0.043, 0.093, 0.140, and 0.174. Circles show data from CMM, solid curves show the total wave train, and dashed curves show the incident wave alone.

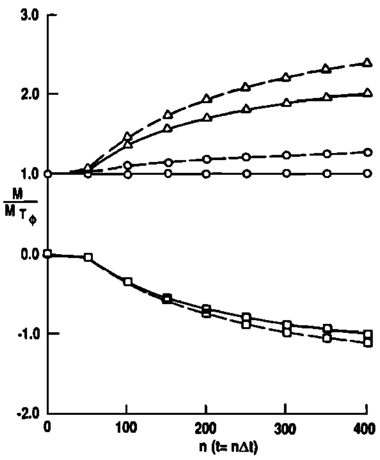

Fig. 7. Total mass in wave train components. Diverging channel. Circles, triangles, and squares show total, incident wave, and reflected wave mass, respectively; solid and dashed curves show mass-conserving and nonconserving equations, respectively.

where b_0 is the initial channel width and H_0 and $H(x)$ are the initial and evolved maximum wave heights. The numerical results reproduce the data well up to 40 water depths beyond the initial measurement station, beyond which the data drop progressively further below the asymptotic - 2/3 slope. This drop in experimental wave height is presumably due to frictional damping.

For the case of a converging channel, the experimental wave height evolves according to a much flatter, - 1/2 slope which mimics a Green's law evolution. The numerical results of CMM reproduce this behavior. CMM offered, as explanation of the - 2/3 and - 1/2 slope discrepancies, an argument based on nonlinear distortion of the linear characteristics in the converging channel case. CMM's results are questioned below, however. It is noted that the numerical results of CMM for the converging channel actually tend to underpredict wave height at large distances from the initial measuring station and thus do not show any accumulating effect of frictional damping. (CMM provide a discussion of the asymptotic wave height resulting from additional damping in the diverging channel case, but do not apply the results to converging channels or provide any explicit computations).

The results of the following two sections indicate that the agreement between data and computations found by CMM in the converging channel case may have been fortuitous, and we thus will concentrate on this point where appropriate.

6.2. Numerical Computations

The mass-conserving RLW equations (37) were used first to compute wave evolution in the converging and diverging channels. Results are shown in Figures 5 and 6. The numerical channels were taken to correspond to the experimental channels as closely as possible; the small tails of constant amplitude on each curve correspond to the constant width entrance channels. In each figure, solid curves correspond to maximum wave height in the combined transmitted-reflected wave system ($\eta = \eta^+ + \eta^-$), while the dashed curves correspond to a transmitted wave alone ($\eta = \eta^+$) when reflection is neglected.

In both the cases of channel divergence and convergence, the wave heights computed from mass-conserving equations evolve largely according to the - 2/3 slope, adiabatic relation. For the diverging channel (Figure 5), these results are in close agreement with CMM's results, with the only deviation between experiment and numerical results being presumably due to the slow accumulation of frictional effects. For the converging channel case, the results here differ markedly from CMM's numerical results and from data, which essentially evolves at a different (- 1/2) slope right from the initial measurement point. These results are initially discouraging, since it is not apparent that the deviation is due to a similar slow accumulation of frictional damping (however, see section 6.3).

Corresponding results were computed using non-conservative RLW equations obtained from (30). The evolution obtained from the nonconservative equations differs markedly from the conservative evolution, with wave heights evolving approximately along a (- 1/2) slope. This leads to (again fortuitous) agreement between data and computations for the converging channel (again with slight underprediction of data at large distances), but significant overprediction of data for the diverging channel case.

The fact that CMM obtained agreement, in the diverging channel, with the - 2/3 slope evolution in the data rather than with the present, non-conservative estimate of a - 1/2 slope, is due in part to their idealization of the channel geometry as a uniform wedge with no uniform entrance channel. Wave height in the idealized channel was initialized according to data from the first measurement point in the model channel, which is located approximately 38 cm back in the uniform 5-cm channel before the junction with the expanding channel, or 225 cm from the virtual origin of the idealized wedge (judging from Figure 2 of CMM). The measured wave is thus placed in a numerical channel ~ 15% narrower than the physical channel and consequently has 15% less total mass than the experimental wave. Using the present nonconservative model with the idealized geometry and the initial measured wave heights at the first measurement point, we obtained numerical results which are in agreement with those presented by CMM. We believe these to be in error because of the idealization of the channel geometry.

We finish here with a discussion of mass balance in the conserving and nonconserving equations. Since the differences between conserving and nonconserving equations lie in terms which are small compared to the orders of magnitude considered in obtaining the original KdV equations, it would be expected that local errors in the nonconserving equations should be small over several wavelengths. This argument does not hold up for the propagation distances considered in the experiments.

In Figures 7 and 8, we show the evolution of total, incident wave, and reflected wave mass with time in the computations described above. Results are for the largest-amplitude cases in each of Figures 5 and 6; since the reflection mechanism is

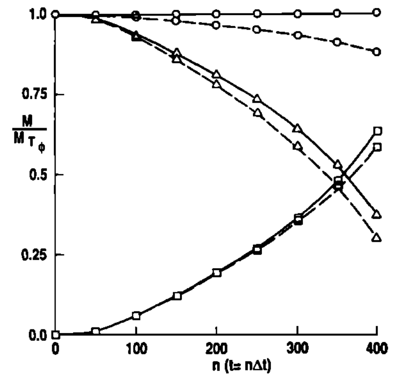

Fig. 8. Total mass in wave train components. (converging channel). Symbols are as in Figure 7.

linear, little variation occurs for different initial amplitudes in each case. For all the computations above, the implicit schemes were run at a Courant number of 1, as suggested by Eilbeck and McGuire [1975]. No attempt was made to optimize accuracy of results by varying grid spacing and Courant number. For the mass-conserving results (indicated by solid lines), total mass was maintained to an accuracy of three significant figures in double precision computations, which is sufficient for the comparisons given here. Deviations in transmitted, reflected, and total mass for the nonconserving results (indicated by dashed lines) are significant for the propagation distances considered. In each case, the majority of deviation from the mass-conserving results is contained in the transmitted wave. These results indicate that the modifications to the basic forms of the equations employed by Miles [1979] to construct mass balance arguments should be incorporated in the governing equations themselves in any practical calculation involving waves in a slowly varying channel.

6.3. Linear Damping Effects

We now consider the effect of a simple linear damping as a possible explanation of the discrepancy between data and numerical results in the previous section. Rather than attempting to obtain a damping coefficient analytically, we posit a simple coefficient β with initially unknown value, and modify the KdV-RLW model equations into the revised forms

$$b\eta^{\pm}_{t} \pm bc\eta^{\pm}_{x} + \dots + \beta(b + 2h)\eta^{\pm} = 0 \qquad (40)$$

The factor (b + 2h) is retained to include the varying effect of channel width and depth (i.e., the relative importance of sidewall and bottom friction) as channel geometry changes. The quantity (b + 2h) is the wetted perimeter of the channel in the linear approximation. The inclusion of the damping term modifies the conclusions on total mass balance. Adding the component equations of (40) and integrating out to $\pm\infty$ yields the expression

$$\frac{d}{dt}\int_{-\infty}^{\infty} b\eta dx = -\beta\int_{-\infty}^{\infty}(b + 2h)\eta dx \qquad (41)$$

The sink term then represents a loss of mass from organized wave motion due to frictional damping of the fluid velocity. This loss of mass would necessarily be absorbed by the stationary (non-wave) water column, leading (at $t\to\infty$) to a distributed increase in depth commensurate with the total initial mass of the organized wave form.

We proceed by examining the largest-amplitude diverging channel case. The value of β is adjusted to obtain reasonable agreement between data and numerical wave height over the entire range of evolution. (This agreement is evaluated purely qualitatively; small changes in β do not significantly alter the results.) On the basis of this procedure, a value of $\beta = 0.004$ is chosen and then is held fixed for the remainder of the computations. Calculations for the three initial amplitudes of the diverging channel case are shown in Figure 9. The linear damping mechanism is successful in representing the gradual accumulation of damping in the diverging channel case.

Turning to the converging channel case, we keep $\beta = 0.004$ and compute the results presented in Figure 10. In this case, linear damping effects accumulate immediately and are seen to account for the general lower slope evolution of the wave height. It is thus apparent that the discrepancy between data and the preferred mass-conserving computations is explainable by simple laminar damping in both the diverging and converging channels, even though the discrepancies accumulate differently. We feel that these results support the validity of the present computations over those given by CMM. There is some indication from the low-amplitude converging channel case that the tuned value of β is somewhat too high. This would be expected, since the converging channel water depth is 50% greater than the diverging channel depth, and thus laminar damping effects would be somewhat reduced.

We remark that a somewhat more standard means of adding a damping term would be to add Burgher's type (second derivative) terms to the equations.

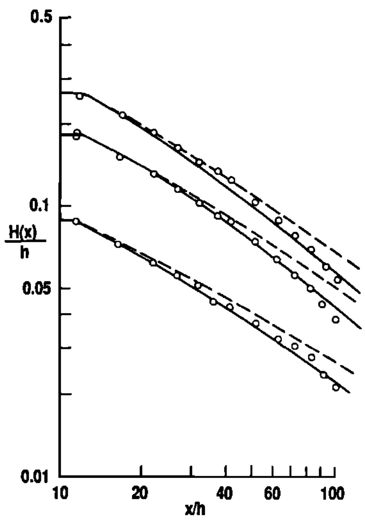

Fig. 9. Linear damping of solitary wave in diverging channel. Conditions are as in Figure 5. Circles show data from CMM, dashed curves show the undamped wave, and solid curves show the damped wave.

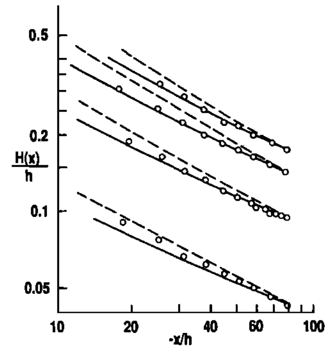

Fig. 10. Linear damping of solitary wave in converging channel. Conditions as in Figure 6. Circles show data from CMM, dashed curves show the undamped wave, and solid curves shown the damped wave.

However, the factors which make this type of damping term appropriate in studying shock dynamics are inappropriate for the application here. In the case of a dissipative shock forming in a nondispersive environment, numerical results become contaminated by high-frequency noise which is essentially a parasitic addition to a low-frequency (infinitely long wavelength) process. The second-derivative damping term concentrates damping in the high-frequency components. In the present case, where well-organized wave motions are present at a range of frequencies in evolved wave fields, experience would indicate that bottom boundary layer damping of high-frequency components should be lower than for low-frequency components, because of increasing relative water depth. The present model distributes damping uniformly over all frequencies; this is not a completely desirable result but is certainly more appropriate than the Burgher's form.

7. Reflection of Time-Periodic Wave Trains by Undular Beds

We now turn to a case where strong reflections arise due to a resonant reflection mechanism. In particular, we study the reflection of a cnoidal wave by a field of sinusoidal bars placed on the bottom of an otherwise uniform channel. This problem has been studied in the linear wave limit by Davies and Heathershaw [1984] and Mei [1985]. Recently, Yoon and Liu [1987] have considered the problem studied here from the point of view of resonant interaction theory, where attention is restricted solely to the interaction of the fundamental Fourier component of the cnoidal wave and the bottom undulation, and all simple shoaling effects are neglected. A more complete set of calculations is provided here which exhibit several physical features which do not arise in the results of Yoon and Liu.

7.1. Evolution Equations for Time-Periodic Waves

Neglecting transverse (y direction) variations, the surface displacements of time-periodic incident and reflected waves governed by (19) may be expressed as a sum of Fourier modes with variable amplitudes:

$$\eta = \sum_{n=1}^{N} \left[\frac{A_n(x)}{2} e^{in(\int k dx - \omega t)} + c.c.\right] \qquad (42a)$$

$$\zeta = \sum_{n=1}^{N} \left[\frac{B_n(x)}{2} e^{in(-\int k dx - \omega t)} + c.c.\right] \qquad (42b)$$

where $\eta = \eta^+$ and $\zeta = \eta^-$ for convenience and c.c. denotes the complex conjugate. Substituting the forms of η and ζ in the coupled KdV equations (19) yields the lowest order coupled evolution equations for the incident wave amplitude

$$A_{n_x} + \frac{h_x}{4h}\left[A_n - B_n e^{-2in\int k dx}\right] - \frac{in^3k^3h^2}{6} A_n + \frac{3ink}{8h}\left[\sum_{\ell=1}^{n-1} A_\ell A_{n-\ell} + 2\sum_{\ell=1}^{N-n} A_\ell^* A_{n+\ell}\right] = 0 \qquad (43)$$

and a corresponding equation for the reflected wave amplitude. These equations represent a more complete model of the wave propagation problem than the final equations employed by Yoon and Liu [1987] to study resonant reflection. Equations similar to theirs are derived in Appendix B, and the effect of using the more complete form (43) is discussed below.

Energy conservation in the reflection process may be analyzed using the coupled evolution equations and is used below as a test of accuracy for the numerical scheme. The conservation law derived from (43) and its counterpart is given by

$$\left[c \sum_{n=1}^{N} |A_n|^2\right]_x - \left[c \sum_{n=1}^{N} |B_n|^2\right]_x = 0$$

or

$$c \left\{ \sum_{n=1}^{N} (|A_n|^2 - |B_n|^2)\right\} = \text{constant} \qquad (44)$$

In the case of a rippled bed in constant mean depth (Figure 11), the conservation equation (44) becomes

$$\sum_{n=1}^{N} (I_n^2 - R_n^2 - T_n^2) = 0 \qquad (45)$$

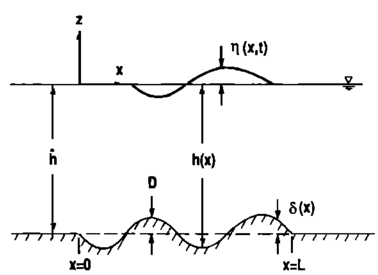

Fig. 11. Geometry of the sinusoidal bed form.

where

$$T_n = \frac{|A_n(L)|}{|A_1(0)|} \quad R_n = \frac{|B_n(0)|}{|A_1(0)|}$$

$$I_n = \frac{|A_n(0)|}{|A_1(0)|} \tag{46}$$

Here, I_n represents a measure of each harmonic amplitude to the fundamental amplitude in the steady incident wave, and R_n and T_n are reflection and transmission coefficients for each mode, normalized by the fundamental incident amplitude.

7.2. Numerical Scheme

Reflections from a rippled bed with periodic sinusoidal depth variations are studied using the evolution equations (43) developed in numerical form. A finite difference scheme centered on $x = (m + 1/2)\Delta x$ is used for the equations, giving

$$\frac{A_n^{m+1} - A_n^m}{\Delta x} + \frac{(h^{m+1} - h^m)}{4\Delta x}\frac{(A_n^{m+1} + A_n^m)}{(h^{m+1} + h^m)}$$

$$- \frac{in^3(k^3h^2A_n)^{m+1}}{12} - \frac{in^3(k^3h^2A_n)^m}{12}$$

$$+ \frac{3in}{16}\left[\left(\frac{k}{h}\sum_{\ell=1}^{n-1} A_\ell A_{n-\ell}\right)^{m+1} + \left(\frac{k}{h}\sum_{\ell=1}^{n-1} A_\ell A_{n-\ell}\right)^m\right.$$

$$\left. + \left(\frac{2k}{h}\sum_{\ell=1}^{N-n} A_\ell^* A_{n+\ell}\right)^{m+1} + \left(\frac{2k}{h}\sum_{\ell=1}^{N-n} A_\ell^* A_{n+\ell}\right)^m\right]$$

$$= \frac{(h^{m+1} - h^m)}{4\Delta x}\frac{(B_n^{m+1}e^{-2in\psi^{m+1}} + B_n^m e^{-2in\psi^m})}{(h^{m+1} + h^m)} \tag{47}$$

and a similar form for the reflected wave component.

The reflected and transmitted waves are obtained by an iterative procedure. First for k=0, using initial values for $A_n(m=0)$ as specified by the permanent cnoidal wave solution, the incident wave (obtained using equation (47)) is marched in x (without considering the reflected wave) using an iterative scheme to linearize the quadratic terms. Then using the present value of the incident wave field along the disturbance, the equations for the B_n are solved by starting at a point downstream of the disturbance where reflection is absent and marching backwards to solve for the reflected wave field. The incident wave and reflected wave are then successively updated until the relative error between two successive solutions (k and k+1) of the reflected and incident wave field is less than a predetermined value ρ, i.e.,

$$\frac{|A_N^m|^{k+1} - |A_N^m|^k}{|A_N^m|^k} < \rho \qquad \frac{|B_1^m|^{k+1} - |B_1^m|^k}{|B_1^m|^k} < \rho \tag{48}$$

where k+1 and k represent the current and the previous iterations. For $\rho = 10^{-4}$, only three iterations are required to obtain solutions of A_n and B_n. The phase $\psi = \int k\,dx$ is calculated using the trapezoidal rule.

7.3. Reflection From a Rippled Bed

For the present numerical calculations, a rippled bed is defined by

$$h = \bar{h} - \delta(x) \qquad 0 < x < L \tag{49}$$

where L is length of the ripple patch, $\bar{h}$ is the constant depth and δ is a small but rapid variation to the depth. Choosing sinusoidal bed variations as in previous works, δ is given by

$$\delta = D\sin\lambda x \qquad 0 < x < L \tag{50}$$

where D is the ripple amplitude and λ is the ripple wave number.

We first consider the propagation of linear waves over the ripple patch. Linear wave reflection from the ripple patch is a function of the number of ripples in the patch, the ripple amplitude and the ripple length. To examine the effects of the ripple length on reflection, calculations are carried out for a wide range of values of the parameter $2K_1/\lambda$, where K_1 is the wave number of the fundamental component of the incident wave, correct to $O(kh)^2$. The parameter $2K_1/\lambda$ is varied by changing the ripple length for a fixed wave number. This approach is preferred to varying wave period for a fixed rippled length because in the latter approach the waves in the short-wave regime (K_1 large) may not satisfy the shallow water scaling. In all the cases analyzed here, waves of period T = 1.8 s in water depth h = 0.1 m are used, corresponding to a value of $\mu^2 = \omega^2 h/g = 0.124$. To study the effect of the number of ripples in the patch, two patches, one consisting of two ripples and another of four ripples, are modeled.

In Figure 12, results for propagation of a linear wave over rippled beds are presented for a ripple amplitude $D/h = 0.4$. All calculations were carried out using a $\Delta x = \pi/20\lambda$ to obtain accurate results at large $2K_1/\lambda$. Resonant Bragg scattering is observed at $2K_1/\lambda = 1$. The conservation law (equation (45)) reduces to

$$R^2 + T^2 = 1 \tag{51}$$

for linear waves. For small ripple amplitudes, the conservation law is satisfied for the entire range of $2K_1/\lambda$ values with errors less than 10^{-3}. For $D/\bar{h} = 0.4$ in the region $0.95 < 2K_1/\lambda < 1.05$ the scheme is not convergent owing to overprediction of the reflection on the first pass. To rectify this problem, the numerical scheme is

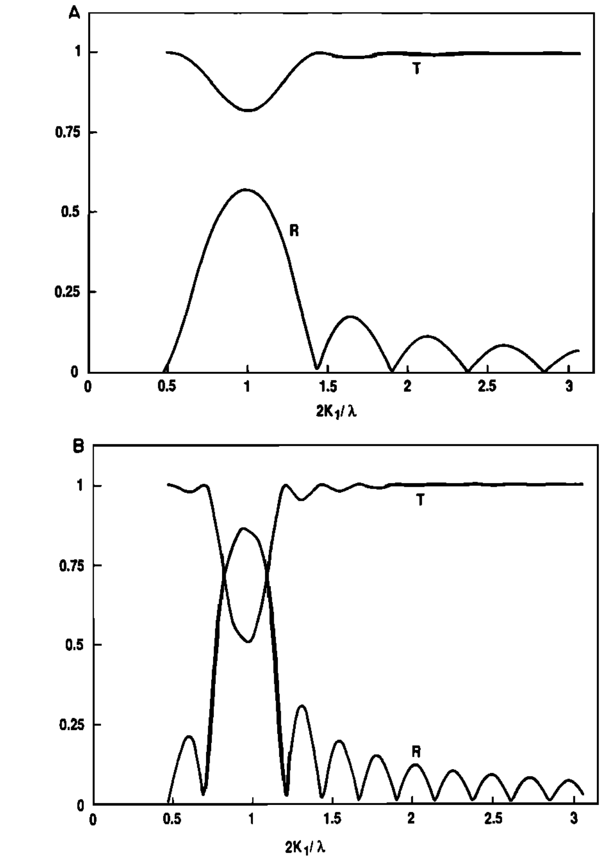

Fig. 12. Variation of reflection and transmission coefficients with $2K_1/\lambda$ for linear waves normally incident on a sinusoidal patch, for (a) n = 2, $D/\bar{h}$ = 0.4 and (b) n = 4, $D/\bar{h}$ = 0.4.

solved by an iterative procedure. First, the incident and reflected wave field for ripple amplitude $D/\bar{h}$ = 0.2 is calculated. Using the calculated wave field as the initial value for the incident and reflected wave fields, the numerical scheme is solved for increasing ripple amplitude with an increment $\Delta D/\bar{h}$ = 0.05, until $D/\bar{h}$ = 0.4 is reached. This approach reduced the errors in the conservation law to less than 10^{-2} for the range $0.95 < 2K_1/\lambda < 1.05$.

Reflection and transmission coefficients R, T are presented as a function of $2K_1/\lambda$ in Figure 12. Figures 12a and b show results for ripple patches containing two and four ripples, respectively. The major effect of increasing the number of ripples, while holding ripple amplitude and water depth constant, is to tune the resonant response of the ripple bed and increase the magnitude of the resonant reflection. These effects are similar to the general trend of results in intermediate depth, as studied by Davies and Heathershaw [1984] and Kirby [1986].

Reflection of nonlinear waves from a rippled bed is next studied. The propagation of a cnoidal wave of period 1.8 s and wave height 0.02 m is considered. In Figure 13a, the reflection and transmission coefficients of the fundamental component (R_1, T_1) as defined in (46) are presented. The ripple amplitude $D/\bar{h}$ = 0.4 and the number of ripples is 2 for this case. There is no appreciable change in the values of reflection coefficient from the linear case, but there is a small shift in the peaks and zeros of R_1 which is presumably due to nonlinear distortion of the incident wave length. In the near-resonance region there is no appreciable change in the transmission coefficient T_1 with respect to the linear result. The total energy transmitted (E_T) and reflected (E_R), normalized with respect to initial energy, are shown as dotted lines. Energy conservation defined by (45) is satisfied with an error $< 10^{-3}$.

We note that in the region of $2K_1/\lambda > 1$, the transmission coefficient of the fundamental component, T_1, experiences a significant drop even though the value E_T indicates that no significant reflection is occurring. In this region the sinusoidal ripples are becoming comparable in length to or longer than the surface wave length, and the surface waves are able to evolve by nontrivial amounts as they shoal over the ripple crests. The reduction of T_1 represents a destabilization of the incident wave, after which energy is transferred to higher harmonics. This effect would not appear in the results of the model developed by Yoon and Liu [1987] where nonresonant shoaling effects are neglected.

We also note a rise in E_R and a drop in E_T as $2K_1/\lambda \to 0.5$. This represents the resonant inter-

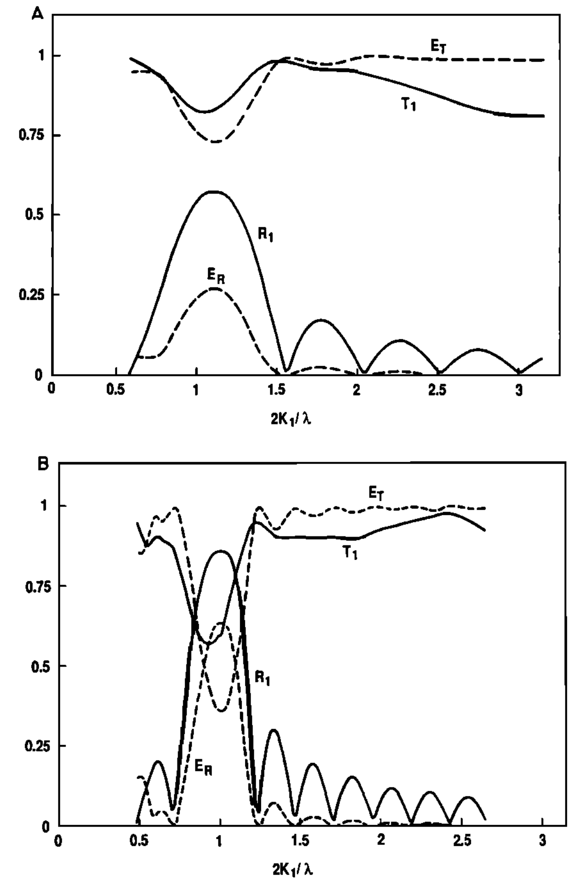

Fig. 13. Variation of reflection and transmission coefficients of fundamental harmonic with $2K_1/\lambda$ for nonlinear wave propagation over a sinusoidal patch for (a) n = 2, $D/\bar{h}$ = 0.4 and (b) n = 4, $D/\bar{h}$ = 0.4. The normalized reflected and transmitted energy E_R and E_T are shown.

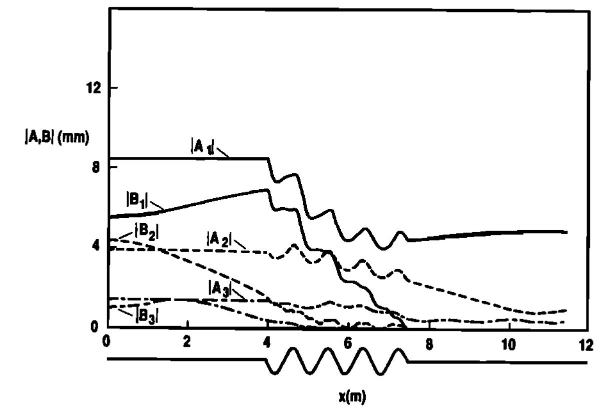

Fig. 14. Variation of component amplitudes of transmitted and reflected waves with x, at Bragg resonance for nonlinear wave propagation over a sinusoidal patch of 4 ripples and $D/\bar{h} = 0.4$ (first three harmonics).

action between the first superharmonic of the wave field and the ripple patch. The modification to the total transmitted energy is then due to the decreasing energy content in the harmonic amplitude.

Figure 13b presents nonlinear results for the patch with four ripples. Differences between linear and nonlinear results are more accentuated than in the two bar case. In the region of resonant reflection, T_1 is greater in the nonlinear case than in the linear case. This result is due to the fact that the transmitted component continually gains energy from its harmonics as it is lost to reflection over the bar field, and thus ends up with a surplus in comparison to the linear case. In contrast, the reflection coefficient R_1 is again little changed from the linear case. The maintenance of a higher value of the incident amplitude $A_1(x)$ over the bar field should lead to greater energy transfer to the reflected wave component $B_1(x)$. This effect is balanced by the fact that the B_1 component loses energy through harmonic generation as the reflected wave height increases, and in the present case, the two effects nearly cancel each other.

After the incident and reflected waves move into the region of constant depth, the waves evolve as they propagate owing to nonequilibrium between the Fourier components of the surface displacement. To illustrate this evolution, the transformation of the component amplitudes of the incident and reflected wave are analyzed for the case of resonant Bragg scattering. In Figure 14, the evolution of the component amplitudes of the incident and reflected wave is presented, for waves propagating over a patch of four ripples, with ripple amplitude $D/\bar{h} = 0.4$. Results were calculated for an initial permanent form wave consisting of 20 harmonics, although only the evolution of the first three harmonics are presented. The loss of energy in harmonics of the incident wave and the gain of energy in the reflected wave harmonics are both apparent. Also apparent is the disequilibrium of the transmitted waves and reflected waves as they leave the area of the ripple patch. This disequilibrium leads to a continuous evolution of the reflected wave and transmitted wave away from the ripple patch. This effect presents serious difficulties in the practical measurement of reflection and transmission, since these quantities are essentially functions of space. (The only spatially uniform quantity would be the energy flux of the reflected and transmitted wave trains.)

8. Conclusions

The present study has developed a scheme for obtaining the linear coupling between opposite going, weakly dispersive long waves due to channel variations in the direction of propagation. The model is shown to predict the generation of a reflected wave quite well in one case where comprehensive data are available.

Computational results have indicated that errors in mass conservation embedded in standard forms of the KdV-RLW evolution equations, which are locally of smaller order than the approximation employed in the equations, nevertheless interfere in numerical integrations over length scales appropriate to existing physical experiments. By extension, these effects would be expected to have serious impacts in field applications. Appropriate mass-conserving forms of the equations have been provided which are accurate to the same degree of approximation as the original equations.

It is noted that the neglect of nonlinear interaction between opposite going waves in this study renders the model inapplicable to the study of details of the head-on collision of solitary waves of comparable amplitude. Derivation of the appropriate coupling terms would represent a valuable addition to the present model. Further, application of the weakly two-dimensional model obtained in sections 2 and 3 would be of value; cases employing only the forward-propagating component will be reported on shortly.

Appendix A: Approximate Angular Relations in K-P Dispersion

The restriction to small angles of propagation implied in the K-P equation may be analyzed by looking at the propagation of a plane wave given by

$$\eta = ae^{i(k\cos\theta x + k\sin\theta y - \omega t)} \tag{A1}$$

The expression $\gamma^2\eta$ in (4) is then given by

$$\gamma^2\eta = \left(\frac{\omega^2}{gh} - k^2\sin^2\theta\right)\eta = k^2(1 - \sin^2\theta)\eta \tag{A2}$$

An expression for $\gamma\eta$ based on the binomial expansion employed in section 2 is then

$$\gamma\eta = k(1 - \sin^2\theta)^{1/2}\eta \approx k\left[1 - \frac{1}{2}\sin^2\theta\right]\eta \tag{A3}$$

which is only valid if $\sin\theta \approx \theta \ll 1$. The direction of wave propagation is thus only allowed to deviate slightly from the preferred x direction.

This scaling distinction may be further understood by comparing the model K-P equations obtained here with the usual parabolic approximation for time-harmonic linear waves. The set of coupled equations (15) in differential form may be compared with the coupled parabolic equations given by Liu and Tsay [1983] by making the substitution

$$\eta^+ = A(x,y)\, e^{i(k_0x-\omega t)}$$

$$\eta^- = B(x,y)\, e^{i(-k_0x-\omega t)} \tag{A4}$$

to yield

$$2ikhA_x + 2kh(k-k_0)A + i(kh)_xA + (hA_y)_y = i(kh)_x\, Be^{-2ikx} \tag{A5a}$$

$$2ikhB_x - 2kh(k-k_0)B + i(kh)_xB - (hB_y)_y = i(kh)_x\, Ae^{2ikx} \tag{A5b}$$

which are essentially similar to the shallow water limits of the coupled parabolic equations of Liu and Tsay [1983, equations (2.12-2.13)].

Appendix B: Simplified Equations for Near-Resonant Reflection

The set of equations (43) represents a general model for reflection of periodic waves from bottom topography h(x) and covers the special case of reflection of waves from a bed of sinusoidal ripples of small amplitude. Yoon and Liu [1986] have provided a more restricted theory for near-resonant interaction (small detuning with respect to the Bragg condition) which neglects contributions to reflection which are far from resonance and which also neglects shoaling effects in each wave component alone. Here, we obtain an analogous dimensional form of the governing equations as a reduction of the general theory (equation (43)).

We consider the depth $h(x)$ to be split into a slowly varying portion $\bar{h}(x)$ and a rapidly varying, small-amplitude portion $\delta(x)$, with $\delta/\bar{h} = O(\alpha)$. The coupling coefficient $h_x/4h$ is then given by (to $O(\alpha)$)

$$\frac{h_x}{4h} = \frac{\bar{h}_x - \delta_x}{4\bar{h}} \tag{B1}$$

Since simple shoaling effects do not lead to resonant reflection, (43) may be rewritten as

$$A_{n_x} - \frac{in^3\bar{k}^3\bar{h}^2}{6} A_n + \frac{3in\bar{k}}{8\bar{h}} \{\sum_{\ell=1}^{n-1} A_\ell A_{n-\ell} + 2\sum_{\ell=1}^{N-n} A_\ell^* A_{n+\ell}\} = -\frac{\delta_x}{4\bar{h}} B_n\, e^{-2in\int\bar{k}dx} + O(\epsilon^2) \tag{B2a}$$

$$B_{n_x} + \frac{in^3\bar{k}^3\bar{h}^2}{6} B_n - \frac{3in\bar{k}}{8\bar{h}} \{\sum_{\ell=1}^{n-1} B_\ell B_{n-\ell} + 2\sum_{\ell=1}^{N-n} B_\ell^* B_{n-\ell}\} = -\frac{\delta_x}{4\bar{h}} A_n\, e^{2in\int\bar{k}dx} = O(\epsilon^2) \tag{B2b}$$

We note here that the wave phase may be written with respect to $\bar{k}$ to $O(1)$. The dispersion term may be eliminated by the transformation

$$A_n\, e^{in\int\bar{k}dx} = A_n'\, e^{i\int K_n dx}\ ;\qquad B_n\, e^{-in\int\bar{k}x} = B_n'\, e^{-i\int K_n dx} \tag{B3}$$

where

$$K_n = n\bar{k}\, \left(1 + \frac{n^2\bar{k}^2\bar{h}^2}{6}\right) \tag{B4}$$

to give

$$A'_{n_x} + \frac{3in\bar{k}}{8\bar{h}} \{\sum_{\ell=1}^{n-1} A_\ell' A_{n-\ell}'\, e^{i\Delta\alpha_{n\ell}^- x} + 2\sum_{\ell=1}^{N-n} A_\ell'^* A_{n+\ell}'\, e^{i\Delta\alpha_{n\ell}^+ x}\} = -\frac{\delta_x}{4\bar{h}} B_n'\, e^{-2i\int K_n dx} \tag{B5a}$$

$$B'_{n_x} - \frac{3in\bar{k}}{8\bar{h}} \{\sum_{\ell=1}^{n-1} B_\ell' B_{n-\ell}'\, e^{-i\Delta\alpha_{n\ell}^- x} + 2\sum_{\ell=1}^{N-n} A_\ell'^* A_{n+\ell}'\, e^{i\Delta\alpha_{n\ell}^+ x}\} = \frac{\delta_x}{4\bar{h}} A_n'\, e^{2i\int K_n dx} \tag{B5b}$$

where the $\Delta\alpha_{n\ell}^{\pm}$ are detuning parameters given by

$$\Delta\alpha_{n\ell}^{\pm} = \frac{1}{2x}\, n\ell\, (\ell\pm n)\int\bar{k}^3\bar{h}^2 dx \tag{B6}$$

Finally, we take the bottom displacement to be given by

$$\delta = \sum_{p=1}^{\infty} \left(\frac{D_p}{2}\, e^{ip\int\lambda dx} + \text{c.c.}\right) \tag{B7}$$

where λ is the characteristic wave number of the bottom undulation. We assume that λ adjusts according to the shoaling effect of the mean slope, i.e., $\lambda/\bar{k}$ = constant. Differentiating (B7) and substituting in (B5) then gives

$$A'_{n_x} + \frac{3in\bar{k}}{8\bar{h}} \{ \sum_{\ell=1}^{n-1} A'_\ell A'_{n-\ell} e^{i\Delta\bar{\alpha}_{n\ell} x}$$

$$+ \sum_{\ell=1}^{N-n} A'_\ell A'_{n+\ell} e^{i\Delta\overset{+}{\alpha}_{n\ell} x} \} =$$

$$= - \frac{ip\lambda D_p}{8\bar{h}} B'_n e^{i\int(p\lambda - 2K_n)dx} \qquad \text{(B8a)}$$

$$B'_{n_x} - \frac{3in\bar{k}}{8\bar{h}} \{ \sum_{\ell=1}^{n-1} B'_\ell B'_{n-\ell} e^{-i\Delta\bar{\alpha}_{n\ell} x}$$

$$+ 2 \sum_{\ell=1}^{N-n} B'^{*}_\ell B'_{n+\ell} e^{-i\Delta\overset{+}{\alpha}_{n\ell} x} \} =$$

$$= \frac{ip\lambda D_p}{8\bar{h}} A'_n e^{-i\int(p\lambda - 2K_n)dx} \qquad \text{(B8b)}$$

where the near-resonant component p is chosen as being that one which minimizes the quantity ($p\lambda - 2K_n$) and thus minimizes the rate of oscillation of the coupling coefficient. Identifying the factor

$$\Delta\beta_{n_p} = \frac{1}{x} \int(2K_n - p\lambda)dx \qquad \text{(B9)}$$

completes the comparisons to Yoon and Liu's model, which is essentially similar to (B8). We further note that the coefficient $\lambda D/8\bar{h}$ is the appropriate shallow water limit of the coefficient derived from Kirby's [1986] intermediate depth theory.

Acknowledgments. This work was supported in its later stages by the Office of Naval Research through contract N00014-86-K-0790.

References

Benjamin, T. B., J. L. Bona, and J. J. Mahony, Model equations for long waves in nonlinear dispersive systems, Philos. Trans. R. Soc. London, Ser.A A272, 47-78, 1972.

Chang, P., W. K. Melville, and J. W. Miles, On the evolution of a solitary wave in a gradually varying channel, J. Fluid Mech., 95, 401-414, 1979.

Davies, A. G., and A. D. Heathershaw, Surface-wave propagation over sinusoidally varying topography, J. Fluid Mech., 144, 419-443, 1984.

Eilbeck, J. C., and G. R. McGuire, Numerical study of the regularized long-wave equation, 1, numerical methods, J. Comput. Phys., 19, 43-57, 1975.

Engquist, B. and A. Majda, Absorbing boundary conditions for the numerical simulation of waves, Math. Comput., 31, 629-651, 1977.

Goring, D. G., Tsunamis - the propagation of long waves onto a shelf, Rep. KH-R-38, W. M. Keck Lab. of Hydraul. and Water Resour., Calif. Inst. of Technol., Pasadena, 1978.

Kadomtsev, B. B., and V. I. Petviashvili, On the stability of solitary waves in weakly dispersive media, Sov. Phys. Dokl., Engl. Transl., 15, 539-541, 1970.

Katsis, C., and T. R. Akylas, On the excitation of long nonlinear water waves by a moving pressure distribution, 2, Three-dimensional effects, J. Fluid Mech., 177, 49-65, 1987.

Kirby, J. T., A general wave equation for waves over rippled beds, J. Fluid Mech., 162, 171-186, 1986.

Knickerbocker, C. J., and A. C. Newell, Reflections from solitary waves in channels of decreasing depth, J. Fluid Mech., 153, 1-16, 1985.

Liu, P. L.-F., and T.-K. Tsay, On weak reflection of water waves, J. Fluid Mech., 131, 59-71, 1983.

Liu, P. L.-F., S. B. Yoon, and J. T. Kirby, Nonlinear refraction-diffraction of waves in shallow water, J. Fluid Mech., 153, 185-201, 1985.

Maxworthy, T., Experiments on collisions between solitary waves, J. Fluid Mech., 76, 177-185, 1976.

Mei, C. C., Resonant reflection of surface water waves by periodic sand bars, J. Fluid Mech., 152, 315-335, 1985.

Miles, J. W., On the Korteweg-deVries equation for a gradually varying channel, J. Fluid Mech., 91, 181-190, 1979.

Peregrine, D. H., Calculations of the development of an undular bore, J. Fluid Mech., 25, 321-331, 1966.

Peregrine, D. H., Long waves on a beach, J. Fluid Mech., 27, 815-827, 1967.

Shuto, N., Nonlinear long waves in a channel of variable section, Coastal Eng. in Jpn., 17, 1-12, 1974.

Su, C. H., and R. M. Mirie, On head-on collisions between two solitary waves, J. Fluid Mech., 98, 509-525, 1980.

Svendsen, I. A., and J. Buhr Hansen, On the deformation of periodic long waves over a gently sloping bottom, J. Fluid Mech., 87, 433-448, 1978.

Vengayil, P., and J. T. Kirby, Shoaling and reflection of nonlinear shallow water waves, Tech. Rep. UFL/COEL-TR/062, Coastal and Oceanogr. Eng. Dep., Univ. of Fla., Gainesville, 1986.

Yoon, S. B., and P. L.-F. Liu, Resonant reflection of shallow-water waves due to corrugated boundaries, J. Fluid Mech., 180, 451-469, 1987.

J. T. Kirby, Coastal and Oceanographic Engineering Department, College of Engineering, 336 Weil Hall, University of Florida, Gainesville, FL 32611.

P. Vengayil, Civil Engineering Department, Massachusetts Institute of Technology, Cambridge, MA 02139.

(Received September 10, 1987; accepted October 23, 1987.)